Light wave states in quasiperiodic metallic structures

Kang Wang*

Laboratoire de Physique des Solides, UMR CNRS/Université Paris-Sud, 91405 Orsay, France

(Received 10 September 2012; revised manuscript received 27 November 2012; published 10 December 2012)

We investigate the light wave states in the octagonal and decagonal quasiperiodic metallic structures by considering their respective approximants at different orders. The mechanisms underlying the light wave behaviors are studied in relation to various structure parameters and configurations. We show that the formation of the first passbands, that delimit the photonic band gaps and determine the plasma gaps, involves only the lowest frequency resonance modes inside the fat tiles, and that light localization occurs due to resonances in high symmetry local centers as well as in the fragments of such centers, formed by the skinny tiles. The structure filling rate affects the localized state frequencies relative to the first passbands, as well as the plasma frequency levels, by modulating the frequency levels of the resonance modes and the widths of the passbands. The results of this study can be generalized to other metallic quasiperiodic and related structures.

DOI: 10.1103/PhysRevB.86.235110 PACS number(s): 42.25.Bs, 61.44.Br

I. INTRODUCTION

More is known about dielectric quasiperiodic (QP) structures than about the metallic ones; still both these structures have potential applications in photonics and interests in fundamental understanding. On one hand, QP structures are capable of sustaining, due to their high degree rotational symmetries, flat frequency bands and more isotropic band gaps as compared to simple periodic structures; metallic structures can be used, moreover, for electromagnetic absorption and emission, and in the design of metamaterials. On the other hand, These nonperiodic yet determinist structures provide instructive examples for investigating light wave behaviors in complex dielectric and metallic media for different structure configurations at various scales.

Indeed, numerous studies on dielectric QP structures are conducted, triggered by the works on simple periodic[1] and random[2] dielectric structures. Investigations show that two-dimensional (2D) octagonal QP structures can indeed sustain flat frequency bands and near isotropic photonic band gaps,[3] with the gap positions determined by the average distance between scatterers.[4] Many other investigations are also reported, among which we can quote band-gap properties,[5–11] light localization and related properties,[10,12–15] structure defect effects,[16,17] laser effects,[18,19] and light emissions.[20,21]

Concerning the metallic structures, it is shown that photonic band gaps can also be obtained in periodic systems,[22,23] and the existence of a plasma gap down to zero frequency is demonstrated for both periodic[24,25] and disordered[26] structures. As far as the QP structures are concerned, attentions are mainly focused, in the case of one-dimensional (1D) QP structures and related metallic particle chains, on the lack of periodicity and the structure self-similarity. Photonic band-gap opening, broadband absorption, and localization are shown to occur in such structures.[27–29] Higher dimensional QP structures differ from the 1D ones by their high degree rotational symmetries. In the 2D case, photonic band-gap opening and defect-related localization in the plasma gap are obtained in Penrose pentagonal structures,[30] and surface plasmon resonances are observed in planar Penrose[31] and dodecagonal[32] metallic structures.

For 2D dielectric QP structures, we have shown in our previous works that the photonic band gaps are determined by the lattice global average order,[4,10] and localized states are formed in high symmetry local centers in the octagonal and decagonal structures[10,13] due to local resonances in relation with both the geometrical and dielectric parameters. A threshold for the localization regime can be defined as a function of these parameters.[15] In this work we investigate comparatively light wave behaviors in octagonal and decagonal metallic QP structures. We focus our attention on the dependance of light resonances on various structure configurations, as well as on the relations between resonance modes. We show that the first passband, that delimits the photonic band gap and determines the plasma gap, is formed from certain specific low frequency local modes. We demonstrate that, like in the dielectric QP structures, light localization occurs at high symmetry local centers as well, though the underlying mechanism is different. We investigate the mechanisms at the origin of these phenomena in relation to various structure parameters to understand the structure effects and their consequences on light wave behaviors.

We consider here the approximants of the octagonal and the decagonal QP structures. The approximants are periodic structures, thus allowing exact resolution of Maxwell's equations. Besides, the approximants locally reproduce their parent QP lattice patterns, so these structures are good candidates for studying local scale effects. Further, the higher the approximant orders, the larger the unit-cell sizes and better the QP lattice patterns are reproduced. The choice of approximants with different orders will allow us to better illustrate the effects of local configurations on light wave behaviors. Finally, low order approximants have the advantage of containing all the structure unities but still displaying relatively simple lattice configurations, making them well adapted for the time-domain method used in this work, and, as we will see below, good complements to the high order approximants in the understanding of the band formation.

II. APPROXIMANT STRUCTURES

The octagonal and decagonal QP lattices display, respectively, 8- and 10-fold global average rotational symmetries

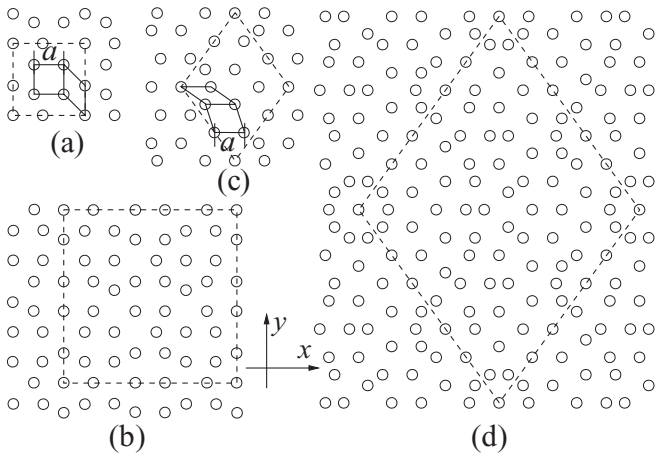

FIG. 1. The 1/1 [(a)] and 3/2 [(b)] approximants of the octagonal QP structure, and the (3/2,5/3) [(c)] and (8/5,13/8) [(d)] approximants of the decagonal QP structure. The lattices nodes are represented by circles and the unit cells delimited by dashed lines. The fat and skinny tiles for each structure family are also outlined (solid lines).

and bond-orientational symmetries. They contain respectively octagonal and decagonal local centers, that belong to their respective maximum global average symmetry groups.

The approximant lattices of these QP lattices studied in this work are displayed in Fig. 1, where the lattice nodes are represented by open circles. The structure unities of these lattices consist of tiles with edge length a. Each structure family contains two kinds of tiles, the fat ones and the skinny ones. Indeed, the octagonal approximants are constructed by square (fat) and $\pi/4$ rhombic (skinny) tiles. They display square unit cells containing, respectively, 7 and 41 tiles, with cell sizes of $a(1+\sqrt{2})$ and $a(3+2\sqrt{2})$. The decagonal approximants are constructed by $2\pi/5$ (fat) and $\pi/5$ (skinny) rhombic tiles. They display unit cells in the form of $2\pi/5$ rhombus, containing, respectively, 11 and 76 tiles, with widths of $a\sqrt{5}\tau^{3-2}$ and $a\sqrt{5}\tau^{5-2}$, and heights of $a\sqrt{5}\tau^{4-1}/\sqrt{1+\tau^2}$ and $a\sqrt{5}\tau^{6-1}/\sqrt{1+\tau^2}$.

The two octagonal approximants can be described as the 1/1 and 3/2 approximants of the octagonal QP lattice, while the two decagonal ones the (3/2,5/3) and (8/5,13/8) approximants of the decagonal QP lattice, in a cut-and-projection description. In fact, these approximants can be obtained, respectively, by approximating $\sqrt{2}$ by 1/1 and 3/2 along the x and y axes, and τ by 3/2 and 5/3, and 8/5 and 13/8, along the x and y axes in respectively the octagonal and the decagonal QP lattices, in the structure formalism proposed for QP alloys.[33,34]

These approximants display, respectively, pseudoglobal average 8- and 10-fold rotational symmetries and octagonal and decagonal bond-orientational symmetries. As mentioned above, higher order approximants better reproduce the parent QC structures. In our case, the 3/2 octagonal and the (8/5,13/8) decagonal approximants are the lowest order ones that reproduce, respectively, the 8- and 10-fold local centers. These local centers are not contained in the 1/1 octagonal and the (3/2,5/3) decagonal approximants (the latter contains only a 5-fold local center in its unit cell). These low order approximants, though displaying simpler lattice configurations, contain nevertheless all the structure unities. Indeed, the 1/1 octagonal approximant contains three fat and four skinny tiles in its unit cell, while the (3/2,5/3) decagonal approximant contains seven fat and four skinny tiles. The comparison of these structures will provide a better understanding of the effects of various structure configurations on the light wave states.

III. BAND STRUCTURES

The metallic structures are formed by scatterers that are infinite high cylinders of perfect metal, of which the dielectric constant is set to negative infinity, placed perpendicular to the lattice plane at the lattice nodes in an air background. Here we consider structures with a filling rate of about 20%, corresponding to a cylinder radius $r = 0.23a$ for these structures, characterized by close lattice node densities [$1.20/a^2$ and $1.21/a^2$ for the 1/1 and 3/2 octagonal approximants, and $1.22/a^2$ and $1.23/a^2$ for the (3/2,5/3) and (8/5,13/8) decagonal approximants, respectively].

Maxwell's equations are solved for TM polarization using a FDTD method. The obtained band diagrams are displayed in Fig. 2. As a matter of fact, the band structures are well resolved for the low order approximants [Figs. 2(a) and 2(c)], thanks to their simple structure configurations. As far as the high order ones are concerned, due to the larger sizes of their unit cells that are characterized by much more complex structural configurations, the band branches are more closely spaced, and there are inevitably unresolved missing states, intrinsic to the time-domain method. However, the band gaps, as well as the photonic states inside the gaps, are well defined [Figs. 2(b) and 2(d)].

Band gaps at lowest frequencies (down to zero) are observed for all these structures. This is comparable to the plasma gaps obtained in periodic and disordered metallic structures.[24–26] It was argued that such a gap is related to a depressed plasma frequency below which a metallic lattice behaves like a homogeneous conducting material. The plasma frequency levels ω_1 for all these structures are listed in Table I.

A photonic band gap, above the plasma gap, is observed for each structure. The characteristics of this gap, i.e., the lower and upper gap edges ω_2 and ω_3, as well as the gap width $\Delta\omega_g$ and mid-gap frequency ω_g, are also given in Table I. Similar to the case of the dielectric structures,[10,13] photonic states (labeled from a to g, with two degenerate states f and f') are found inside the photonic band gaps. As will be discussed below, these states are related to certain local resonance effects that do not affect the band formation.

We notice that both the plasma gap and the photonic band gap are much more isotropic for the high order approximants. This can also be compared to the case of the dielectric structures,[4,10] and is a natural consequence of the approximants approaching perfect QP structures with increasing order.

For each structure, these gaps delimit the lower and upper edges, ω_1 and ω_2, for the first passband (which includes, in the case of the 1/1 octagonal approximant, the three lowest band branches), and the lower edge ω_3 for the second passband. These values are very close for the approximants of each QP structure, with relative differences of the magnitudes of

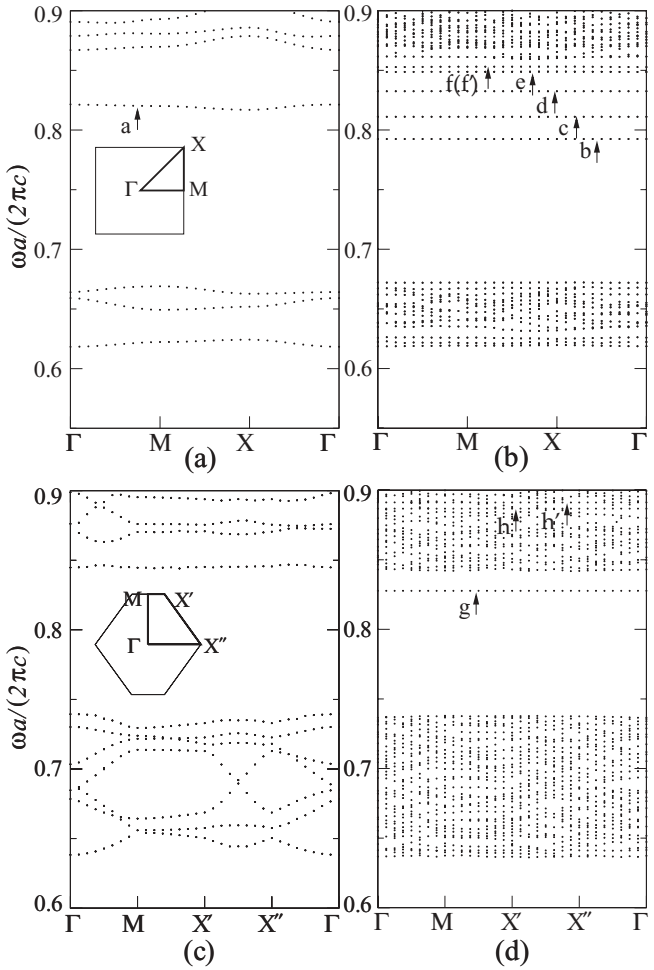

FIG. 2. The band diagrams for the 1/1 [(a)] and 3/2 [(b)] octagonal approximants, and the (3/2,5/3) [(c)] and (8/5,13/8) [(d)] decagonal approximants. Photonic states inside the photonic band gaps are labeled from a to g, two almost degenerate states inside the second passband for the (8/5,13/8) decagonal approximant, h and h', are also indicated in (d).

10^{-3}, indicating the same origin for the band formation. For simplicity, let us consider the first passband, of which the mid-frequency ω_b and width $\Delta\omega_b$ are also listed in Table I.

As mentioned above, these approximant structures are constructed by structure unities that are fat and skinny tiles (Fig. 1). In fact, for the frequency ranges of the first passbands, all the structure unities are not involved in the band formation. To illustrate this, let us first consider the two low order approximants, of which the structure simplicity allows well resolved band structures [Figs. 2(a) and 2(c)]. Indeed, as shown in Fig. 3 for the lowest and the highest branches of the first passbands for these two approximants [Figs. 3(a)–3(d)], the electric fields are essentially confined inside the fat tiles (square and $2\pi/5$ rhombic tiles, respectively), instead of being uniformly distributed in the spaces between the metallic scatterers. As far as the two higher order approximant structures are concerned, their field distributions can also be probed in spite of the lattice structure complexity. Indeed, Figs. 3(e) and 3(f) display the field distributions resulted from the excitation of a Gaussian source with center frequency ω_b

TABLE I. The plasma frequencies ω_1, the lower edges ω_2, the upper edges ω_3, the widths $\Delta\omega_g$ and the mid-frequencies ω_g of the photonic band gaps, as well as the widths $\Delta\omega_b$ and the mid-frequencies ω_b of the first passbands for the (1/1) and (3/2) octagonal and the (3/2,5/3) and (8/5,13/8) decagonal approximants. The eigenfrequencies of the TM_{11} resonance modes $\omega_{TM_{11}}$ inside the square and the $2\pi/5$ rhombic tiles of respectively the octagonal and decagonal approximants, and the corresponding wavelengths $\lambda_{TM_{11}}$ are also listed. All the frequency values are normalized according to $\omega a/2\pi c$, the wavelengths are given in a.

	Octagonal		Decagonal	
	1/1	3/2	(3/2,5/3)	(8/5,13/8)
ω_1	0.618	0.619	0.638	0.636
ω_2	0.669	0.672	0.740	0.738
ω_3	0.867	0.861	0.845	0.843
$\Delta\omega_g$	0.198	0.189	0.106	0.105
ω_g	0.768	0.767	0.792	0.790
$\Delta\omega_b$	0.051	0.053	0.102	0.102
ω_b	0.644	0.645	0.689	0.687
$\omega_{TM_{11}}$	0.644		0.690	
$\lambda_{TM_{11}}$	1.55		1.45	

(see Table I) and a frequency width of $\Delta\omega = 0.2$ (in $\omega a/2\pi c$ unity), in respectively the 3/2 octagonal and the (8/5,13/8) decagonal approximants. We can see that the electric fields are essentially distributed inside the fat tiles as well. This indicates that only the modes in the spaces insides the fat tiles are excited for all these structures in the frequency ranges of the first passbands, and involved in the band formation.

This is not surprising if we consider that the resonance modes occurring inside an individual tile, formed by metallic cylinders at its vertices, have their wavelengths scaling with the tile size. And low frequency modes (in the frequency ranges of the first passbands) can only be supported by the fat tiles. In fact, as shown by the field patterns in Fig. 4, the resonance modes inside these fat tiles, of widths w_f and heights h_f, can be viewed as cavitylike modes, with, roughly, the tile inner diagonals $w_f - 2r$ and $h_f - 2r$ as cavity sizes. For a perfect rectangular cavity of the same sizes, the eigenfrequency for the lowest frequency TM mode $\omega_{TM_{11}} = a\sqrt{1/(w_f - 2r)^2 + 1/(h_f - 2r)^2}/2$ (in $\omega a/2\pi c$ unity). In the present case, the tiles are not perfect square and rectangular cavities, resonance modes inside these structures are obtained by solving the Maxwell's equations. We obtain the eigenfrequencies for the TM_{11} resonance modes for respectively the square and the $2\pi/5$ rhombus tiles, with the same geometrical parameters as in the approximant structures (cylinder radius $r = 0.23a$), $\omega_{TM_{11}} = 0.644$ and 0.690 (in $\omega a/2\pi c$ unity), that are effectively in the frequency ranges of the first passbands of their corresponding approximant structures.

It is worth further considering these eigenfrequency values in relation to the characteristics of the first passbands in more detail. In fact, as shown in Table I, both the band widths $\Delta\omega_b$ and the center frequencies (the band positions) ω_b are very close for the approximants of each QP structure. Moreover, the center frequencies ω_b for the octagonal and decagonal approximants are almost identical to the eigenfrequencies of the first resonance mode $\omega_{TM_{11}}$ inside, respectively, the square

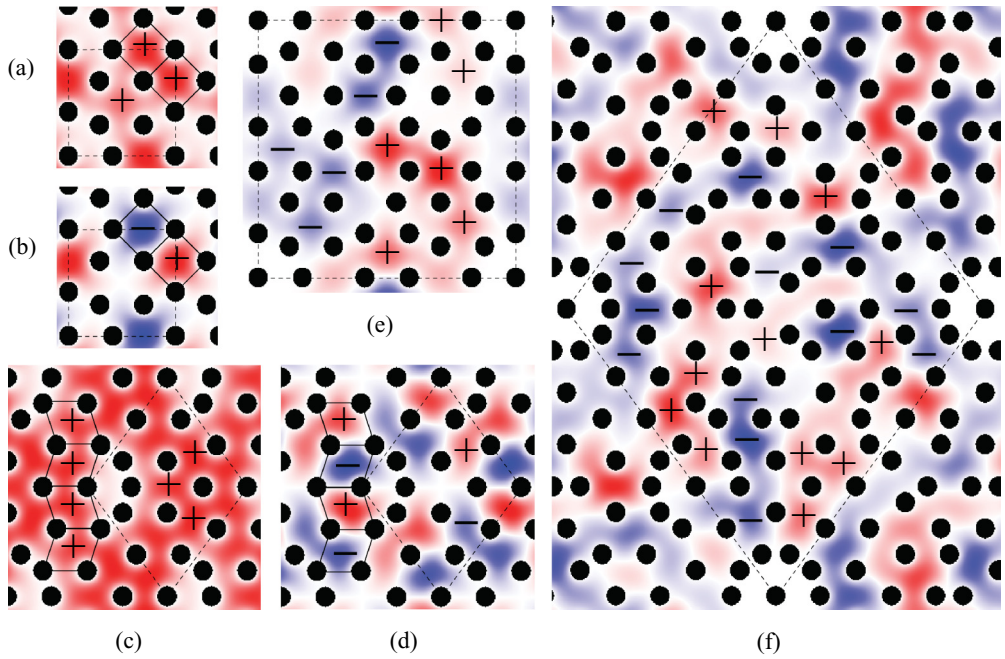

FIG. 3. (Color online) Electric field distributions at Γ point for the lowest [(a) and (c)] and the highest [(b) and (d)] branches of the first passbands for respectively the 1/1 octagonal and the (3/2,5/3) decagonal approximants, as well as those resulted from a Gaussian source with center frequency ω_b (Table I) and a frequency width of 0.2 ($\omega a/2\pi c$) in respectively the 3/2 octagonal [(e)] and the (8/5,13/8) decagonal [(f)] approximants. The fat tiles for each structure family are outlined by solid lines, and the unit cells by dashed lines. The "+/−" signs indicate the field polarities.

and $2\pi/5$ rhombus tiles. Therefore, the upper and lower edges of the first passbands, ω_2 and ω_1, can be related approximately to the eigenfrequencies $\omega_{TM_{11}}$ by the following relation for all these structures:

$$\begin{bmatrix} \omega_2 \\ \omega_1 \end{bmatrix} \approx \omega_{TM_{11}} + \begin{bmatrix} \frac{1}{2}\Delta\omega_b \\ -\frac{1}{2}\Delta\omega_b \end{bmatrix}. \quad (1)$$

This relation corresponds to the typical situation for weak coupling between TM_{11} modes, where the band position is determined by the eigenfrequency of the TM_{11} mode, and the band width by the coupling between these modes, measured by the transfer integrals if a tight binding model is used. This, together with the field distributions in Fig. 3, where the field patterns for the lowest band branches [(a) and (c)] and those for the highest ones [(b) and (d)] are comparable to respectively the bonding and antibonding states between TM_{11} modes in neighbor fat tiles, corroborates the above proposition that the first passbands are formed by interaction between the low frequency modes inside the fat tiles.

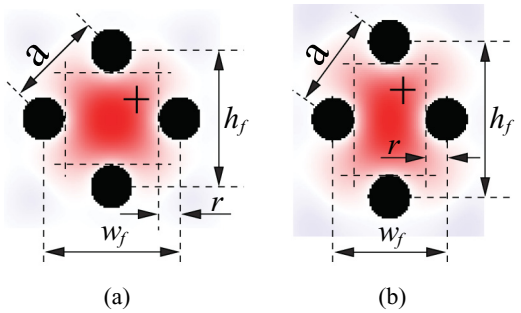

FIG. 4. (Color online) A square [(a)] and a $2\pi/5$ rhombic [(b)] tile, both formed by four metallic cylinders at their vertices. The electric field distributions corresponding to the TM_{11} resonance modes inside these tiles are also shown. The "+/−" signs indicate the field polarities.

This point can further be checked by considering the number of branches in the passbands. As a matter of fact, if the passbands are formed by the TM_{11} modes inside the fat tiles, the number of branches in each passband should equal the number of TM_{11} modes, i.e., the number of fat tiles, contained in the unit cell. Although, as mentioned above, the structure complexity of the two high order approximants prevents us from obtaining all the band branches, intrinsically to the time-domain method used in the present work; this can indeed be checked with the two low order ones. As a matter of fact, there are respectively three and seven branches in the passbands for the 1/1 octagonal and the (3/2,5/3) decagonal approximants, while the two structures contain respectively three and seven fat tiles in their unit cells, satisfying the band-branch number condition.

The band formation at low frequencies is thus selective, involving only the lowest frequency cavitylike resonance modes inside the fat tiles, and the light propagation in the corresponding frequency ranges is realized through the interaction between these modes. The skinny tiles do not contribute directly to the band formation, since, on one hand, they can not sustain cavitylike modes like the fat tiles, as their edge lengths a are much larger than their widths; on the other hand, rectangular cavities of the sizes of the skinny tiles are too narrow to sustain resonance modes in the frequency ranges

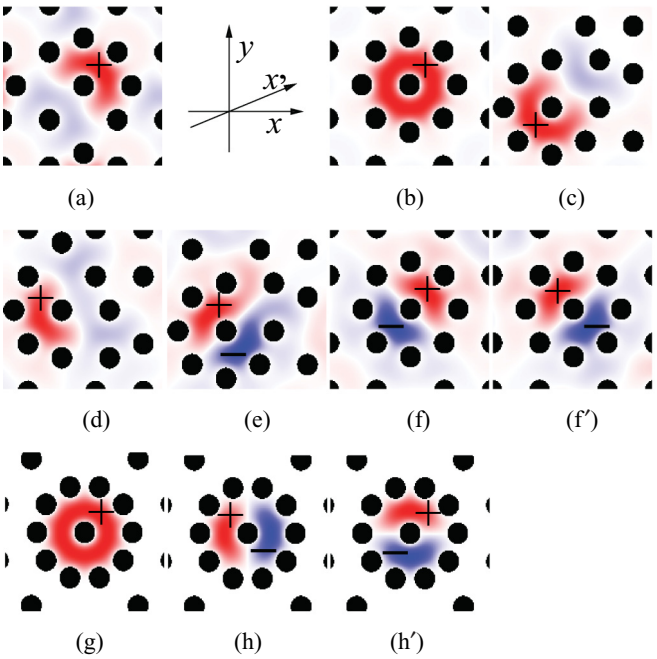

FIG. 5. (Color online) Electric field patterns for the localized states inside the photonic band gaps (a to g), as well as two almost degenerate states in the second passband of the (8/5,13/8) decagonal structure (h and h'). The patterns are lettered following the band labeling in Fig. 2. The "$+/-$" signs indicate the field polarities.

of the first passbands. The skinny tiles can however affect the interaction between the resonance modes in the fat tiles by modulating the distances between the latter.

IV. LIGHT LOCALIZATION

As mentioned above, the band diagrams (Fig. 2) show the existence of photonic states, labeled from a to g, inside the band gaps of the 1/1 and 3/2 octagonal approximants and that of the (8/5,13/8) decagonal approximant. The corresponding electric field patterns are displayed, using the same labels, in Fig. 5, (f and f' being two degenerate states), together with those corresponding to two almost degenerate states, h and h', inside the second passband of the (8/5,13/8) decagonal approximant. The frequency values of these states at Γ point ω_l are listed in Table II.

The electric field patterns show clearly that these states are localized. Indeed, the field patterns of b, f and f' and g, h and h' are confined in the respective maximum symmetry (8- and 10-fold) local centers of the octagonal and decagonal structures, formed by an octagonal or decagonal ring surrounding a central scatterer. The other patterns are confined in local structures that can be considered as parts of the 8-fold local center, formed by a central scatterer and a fragment of the octagonal ring (a and c to e). The localization is corroborated by the flatness of the corresponding frequency bands in Fig. 2. We notice, however, that band a is curved around X point, though the mode a is locally confined. This can be attributed to interaction between localized modes in neighbor unit cells that are small for the 1/1 approximant. This localization phenomenon can be compared to the case of the dielectric QP structures that we studied previously,[10,13,15] where localization occurs intrinsically in the maximum symmetry local centers, as well as in the fragments of such centers, without implying either structure defects or disorders. However, as we will show below, the underlying mechanism in the metallic QP structures is fundamentally different from that in the dielectric ones.

As a matter of fact, in the present case, the field is confined between the octagonal or decagonal rings (or broken rings) and the central scatterer. The field distributions correspond to resonance modes, that occur in the local spaces delimited by these scatterers. To further investigate this point, let us consider isolated individual structures formed by a central scatterer surrounded by octagonal and decagonal rings, as well as broken octagonal rings, with the same geometrical parameters (a and r) as in the approximant structures. Resonance modes inside such individual structures are obtained by solving the Maxwell's equations. We get for these structures the same field patterns as those in the approximant structures shown in Fig. 5. The corresponding resonance frequency values ω_r are listed in Table II as well. Indeed, the same local structure configurations lead to resonance modes with very close frequency values, $\omega_r \approx \omega_l$. This shows that the modes in Fig. 5 are indeed local resonance modes sustained by the local structure patterns. It is worth pointing out that, though there are broken 10-fold local centers in the decagonal approximants, the modes inside these local structures have their frequency levels in the second passbands and are mixed with extended states.

Similar to the case of the fat tiles discussed above, the field distributions of these modes suggest local cavitylike effects. To further illustrate this point, let us give an approximate analytical description to the simplest and most significant cases, i.e., the resonance modes inside the perfect rings. Let ρ be the radial coordinate with its pole on the central cylinder axis. As shown in Fig. 6 in the cases of modes b and g, the electric field magnitude falls to zero at the central cylinder surface $E_z|_{\rho=r} = 0$, and in the vicinity of the surrounding rings $E_z|_{\rho\sim\text{ring}} = 0$. The later condition can be approximately replaced by $E_z|_{\rho=R} = 0$, with R the effective inner radius of the rings. In fact, this simplification consists of approximating

TABLE II. The frequencies of the localized states ω_l at Γ point lettered using the same labels as in Figs. 2 and 5, the resonance frequencies in isolated individual structures ω_r, and the wavelengths λ_r corresponding to ω_r. Frequencies are normalized to $\omega a/2\pi c$. Wavelengths are given in a.

	a	b	c	d	e	f	f'	g	h	h'
ω_l	0.821	0.792	0.811	0.832	0.848	0.853	0.853	0.824	0.885	0.888
ω_r	0.825	0.792	0.813	0.831	0.851	0.854	0.854	0.824	0.885	0.888
λ_r	1.21	1.26	1.23	1.20	1.18	1.17	1.17	1.21	1.13	1.13

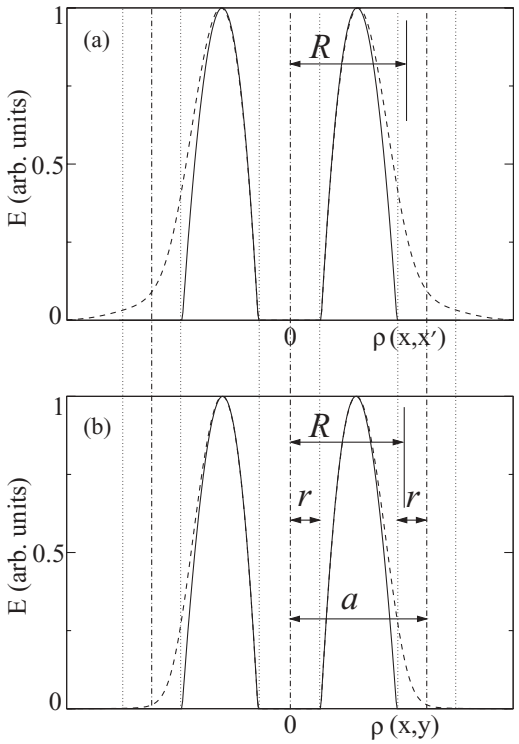

FIG. 6. Normalized electric field distributions for modes b [(a)] and g [(b)] (Fig. 5), in slices passing through the ring center along the x (solid line) and x' (at $\pi/8$) (dashed line) axes [(a)] and along the x (solid line) and y (dashed line) axes [(b)], respectively. The vertical dashed-dotted lines represent the cylindrical scatterer axes. The scatterer cross sections along the x axis are delimited by the dotted lines. Various length parameters are also presented.

the original field pattern symmetry, which is that of the ring, by a cylindrical one. This can be justified by the high degree symmetry of the rings. In fact, the electric field magnitude falls to zero at $\rho = a - r$ when ρ passes through the axis of a cylinder on the ring [along the x axis in Figs. 5(b) and 5(g)], while it displays a Gaussian-like tail beyond $\rho = a - r$ when ρ passes between two neighbor cylinders [along the x' axis in Fig. 5(b) and along the y axis in Fig. 5(g)]. The cylindrical boundary condition approximation neglects this difference. It is obvious that higher symmetry degree leads to a better approximation, as exemplified by the field distributions of modes b and g; the Gaussian-like tail is reduced in the latter case.

Using the above simplified boundary conditions, the resonance frequencies are determined by the classical characteristic equation:

$$J_m(kR) - \frac{J_m(kr)}{N_m(kr)} N_m(kR) = 0 \tag{2}$$

where J_m and N_m are the mth order Bessel and Neumann functions, respectively. Eq. (2) defines a series of resonance modes TM_{mn}, corresponding to the nth roots of Eq. (2) at mth order.

The field patterns b and g display the topology of the TM_{01} mode (no node in neither the angular nor the radial directions), while the patterns f and f', and h and h', display that of the TM_{11} mode (two nodes in the angular direction). And we can check that the resonance frequency values for these modes (b, f, f' and g, h, h') given in Table II correspond effectively to the first roots of Eq. (2) for a well defined R value for each structure. Indeed, for the octagonal one

$$\begin{bmatrix} \omega_b \\ \omega_{f(f')} \end{bmatrix} \approx \begin{bmatrix} \omega_{01} \\ \omega_{11} \end{bmatrix} \tag{3}$$

for $R = 0.84a$; while for the decagonal one

$$\begin{bmatrix} \omega_g \\ \omega_{h(h')} \end{bmatrix} \approx \begin{bmatrix} \omega_{01} \\ \omega_{11} \end{bmatrix} \tag{4}$$

for $R = 0.82a$.

This shows that these resonance modes can indeed be described as cavitylike modes, with approximate cylindrical boundary conditions. For given geometrical configurations (a, r and the symmetry), the eigenfrequency levels can be estimated through a unique parameter R. We notice that R satisfies the relation $(a - r) < R < a$ in both cases, and the R value for the decagonal structure is shorter than that for the octagonal one, due to the shorter interscatterer distance, that is the width of the skinny tiles w_s, on the ring, leading to a better field confinement and higher frequency levels for the cavitylike resonance modes.

The comparison with local centers of lower symmetry degree allows us to probe the condition for such resonances. Here the resonances occur in the maximum symmetry local centers that are formed by skinny tiles, for which the widths w_s are shorter than the local center size a. The 5-fold local centers contained in both the (3/2,5/3) and (8/5,13/8) decagonal approximants are formed by $2\pi/5$ fat tiles, with width w_f larger than a. They do not support such resonance modes.

The resonance condition can thus be expressed through the relation between the local center size a and the interscatterer distance l on the ring. A local center behaves in a cavitylike way for $l < a$. Indeed, the wavelength of a cavitylike mode λ scales with the cavity size $a - 2r$. The resonance modes can be efficiently confined inside the rings for wavelengths much larger than the widths of the space gap between neighbor scatterers, $l - 2r$, on the rings. For the 8- and 10-fold local centers, $l = 0.765a$ and $0.618a$, and, as listed in Table II, $\lambda \gg l - 2r = 0.31a$ and $0.16a$. The energy loss of the local centers increases with l, and cavitylike resonances can no more be sustained for $l > a$ (in any way, a local center can no more be considered as cavity if the interscatterer distance on the ring is larger than the local center size), as in the case of the 5-fold local centers for which $l = w_f = 1.176a$, and no cavitylike resonance modes are obtained.

It is however possible to introduce cavitylike resonances into the 5-fold local centers, and, at the same time, check the validity of the above resonance condition. Let us consider the (3/2,5/3) decagonal approximant. We remove the central scatterer in the 5-fold local center, indicated by the arrow in Fig. 7(a), so that the resulting local center size is $2a > l$ [see the structure in Fig. 7(b)], satisfying the resonance condition. Indeed, a localized state is obtained in this center, as shown by the field pattern in Fig. 7(b). The corresponding state in the band diagram, labeled as i [Fig. 7(c)], has its frequency level $\omega_i = 0.421$ ($\omega a/2\pi c$), and is deeply situated in the plasma gap. Its wavelength, $\lambda = 2.38a$, is much larger than $l - 2r = 0.72a$.

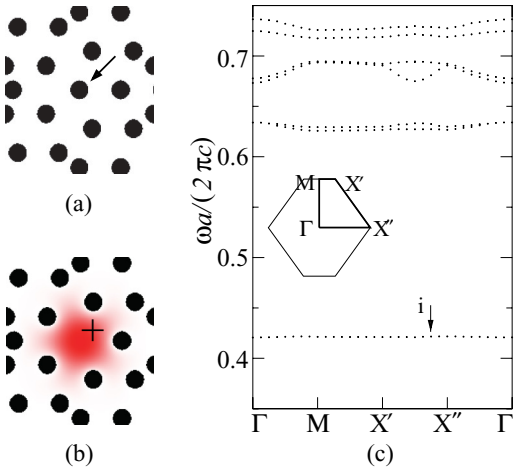

FIG. 7. (Color online) The removal of the center scatterer [indicated by the arrow in (a)] in the 5-fold local center leads to a defect [(b)] in the (3/2,5/3) decagonal approximant, that sustains a local resonance mode [electric field patterns in (b)], with its frequency level in the plasma gap, labeled as i [(c)]. The "$+/-$" signs indicate the field polarities.

This resonance mode can also be described analytically using the above approximation. With the central cylinder absent, we have the only approximate boundary condition

$$E_z|_{\rho=R} = 0. \tag{5}$$

The resonant frequencies are just determined by the roots of

$$E_z = J_m(kR) = 0 \tag{6}$$

The field pattern in Fig. 7(b) corresponds to the TM_{01} mode. The resonance frequency, $\omega_i = 0.421$, corresponds to the root ω_{01} for $R \approx 0.91a$, larger than the R values in the cases of the 8- and 10-fold local centers. The cylindrical boundary condition approximation is less good since the symmetry degree of the local center is lower, and the interscatterer distance is larger on the pentagonal ring.

V. DISCUSSION

The two families of metallic structures studied in the present work, the octagonal and decagonal ones, are both constructed upon two families of structure unities, the fat and the skinny tiles. These tiles play different roles on the light wave behaviors, in particular, on the first passband formation and the light localization.

The first passbands are formed by the coupling between the lowest frequency resonance modes inside the fat tiles, of which the sizes and spatial distributions determine the first passband positions and widths, which determine, in turn, the lower edges of the photonic band gaps. This sheds, besides, new light on the plasma gaps, as the plasma frequencies correspond to the lower edges of the first passbands ω_1, thus depend on the fat-tile configurations as well. In this framework, the plasma gaps are natural consequences of the coupling between the specific lowest frequency modes in these structures.

The slight but noticeable photonic-band-gap width decreases passing from lower to higher order approximants (Table I) can also be explained in this framework. Our results suggest that the widths of the passbands are determined by the coupling between resonance modes formed inside the structure unities. With increasing order, the approximants reproduce better the local structure patterns of their parent QP lattices, approaching thus the average rotational symmetry of the latter at larger local scales. A resonance mode can therefore be surrounded by more near-neighbor modes (not necessarily limited to the first neighbor ones) to which it can couple, increasing the widths of the passbands and, thus, decreasing that of the photonic band gap. This is notably relevant when beginning from the lowest order approximants, that can only reproduce the QP lattice patterns at minimum local scales, such as the first (the 1/1) approximant of the octagonal structure.

Light localization can be described as cavitylike resonance modes inside local structures formed by skinny tiles. The localization is favored by high degree symmetry, that implies short interscatterer distance l on the ring, and by high structure filling rate as well, since a weaker width for the interscatterer space gap on the ring, $l - 2r$, leads to a better confinement.

The filling rate of 20% is rather high for these structures, the scatterer diameter being about three quarters of the shortest interscatterer distance w_s in the decagonal structures. It is interesting to further probe the relation between the localized states and the first passbands for lower structure filling rates.

As mentioned above, the position of the first passband for each structure is determined by the frequency of the cavitylike mode TM_{11} inside the fat tiles [Eq. (1)], and the wavelength for such a mode scales with the cavity width $w_f - 2r$. TM_{11}

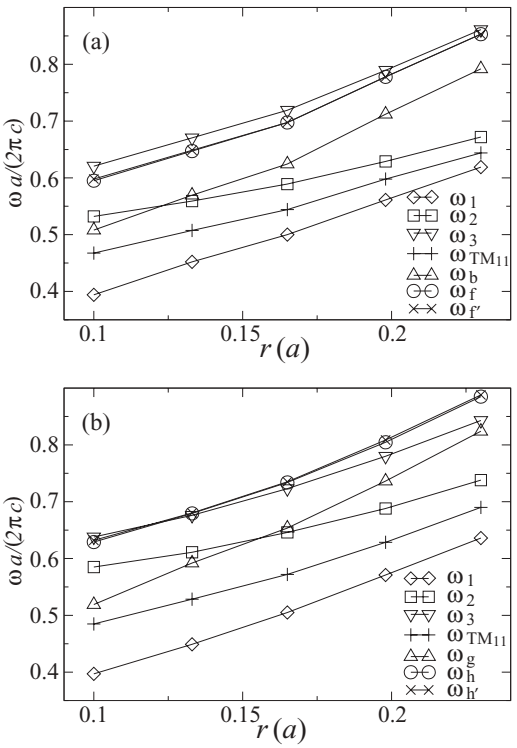

FIG. 8. The lower and upper edges of the first passband, ω_1 and ω_2, the fat-tile resonance mode frequencies $\omega_{TM_{11}}$, the localized mode frequencies in the maximum symmetry local centers ω_b, $\omega_{f(f')}$ and ω_g, $\omega_{h(h')}$, together with the lower edges of the second passbands ω_3, as functions of the scatterer radius r for respectively the 3/2 octagonal [(a)] and the (8/5,13/8) decagonal [(b)] approximants.

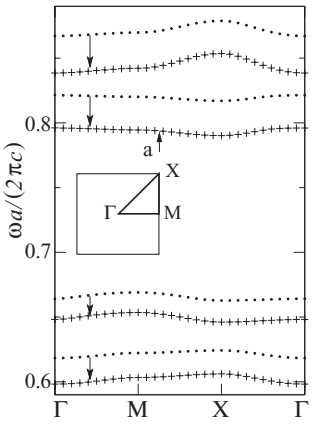

FIG. 9. The photonic band gap and the upper edge of the plasma gap, together with localized state a, obtained for the 1/1 octagonal approximant for a dispersive metal with $\omega_p = 10(\omega a/2\pi c)$ ("+"), compared to those in Fig. 2(a) ("·"). For clarity, only the branches at the gap edges are plotted.

will be shifted to low frequencies for decreasing filling rate. Besides, the coupling between the TM_{11} modes will increase with decreasing filling rate, since these modes will become more spatially extended for increasing space-gap width, $a - 2r$, on the tile edges, leading to the passband width increase.

For a localized state, the wavelength scales with the cavity size $a - 2r$. Here a is shorter than the fat tile width w_f, and the frequency levels of the localized states are above the first passband. The localized state frequencies will be shifted to low frequencies as well for decreasing filling rate. And their differences with $\omega_{TM_{11}}$ will decrease, as the difference between $a - 2r$ and $w_f - 2r$ decreases with decreasing r. Therefore, with decreasing filling rates, the localized states will approach the first passbands and eventually fall inside the latter.

The evolution of the passbands and the localized states following the structure filling rate is illustrated by Fig. 8, where several frequency levels for the two high order approximants are plotted as functions of the scatterer radius r, for r down to $0.1a$ (corresponding to a filling rate of about 4%). Effectively, all the frequency levels are shifted to lower values with decreasing filling rate, and the first passband widths are larger. We notice that Eq. (1) remains satisfied down to the lowest filling rates. Moreover, the frequency levels of the localized states approach those of TM_{11}, and, for the lowest filling rates, the levels of ω_b and ω_g fall inside the first passbands, while those of ω_h and ω_h' for the (8/5,13/8) decagonal approximant are shifted down into the band gap.

It is worth pointing out that perfect metal, with negative infinity dielectric constant, is used to model the metallic structures in this work. This is a good approximation at frequency ranges well below the plasma frequency of the electron gas in the metallic material ω_p. Corrections to the band frequencies will be introduced if metallic dispersion is taken into consideration, especially for higher frequency ranges. Let us illustrate this aspect in the case of the 1/1 octagonal approximant by using a lossless Drude model, with the metallic dielectric constant $\epsilon(\omega) = 1 - {\omega_p}^2/\omega^2$. The photonic band gap, the upper edge of the plasma gap, as well as the localized state inside the photonic band gap, obtained for a dispersive metal with plasma frequency $\omega_p = 10(\omega a/2\pi c)$, are displayed in Fig. 9, together with those obtained for the dispersiveless perfect metal. It is obvious that, due to the metallic dispersion, the band branches are all shifted to low frequencies. The photonic band gap becomes slightly more anisotropic, and its width is reduced as well. These are natural consequences of the reduction of the absolute value of the dielectric contrast between the metallic scatterers and the air background following the frequency. The perturbation of the light wave by the scatterers is weaker, implying, for the resonance modes inside the structure unities, lower eigenfrequencies and more extended spatial distributions, leading to lower positions and larger widths for the passbands with less flat band branches.

Finally, the analysis in the present work shows the intimate relations between the physical properties and geometrical parameters in the metallic approximant structures. Moreover, the results obtained on the approximant structures can be generalized to their parent QP structures, since, on one hand, the existence of different families of structure tiles and high symmetry local centers are characteristics common to both the QP lattices and approximants of sufficiently high orders, and, on the other hand, approximants reproduce locally their parent QP structures, and the properties studied in the present work are essentially determined by local scale effects. Finally, the present results can be generalized to other metallic QP and related structures containing different structure unities and local centers.

VI. CONCLUSION

In summary, light wave states in octagonal and decagonal quasiperiodic metallic structures, that display different long range orders and local configurations, are comparatively studied through their respective approximant structures of various orders. Mechanisms underlying the formation of the first passbands, that separates the photonic band gaps and the plasma gaps, and the light localization in high symmetry local centers are investigated and discussed. This study shows the particularities of metallic structures constructed upon different families of structure components, by analyzing the contributions of different structure unities to the band formation, localization, as well as the plasma gap opening. The effects of local symmetry and structure filling rate are discussed as well. The results and analysis can be generalized to other metallic quasiperiodic and related structures.

*kang.wang@u-psud.fr

[1]E. Yablonovitch, Phys. Rev. Lett. **58**, 2059 (1987).
[2]S. John, Phys. Rev. Lett. **58**, 2486 (1987).
[3]Y. S. Chan, C. T. Chan, and Z. Y. Liu, Phys. Rev. Lett. **80**, 956 (1998).
[4]K. Wang, S. David, A. Chelnokov, and J.-M. Lourtioz, J. Mod. Opt. **50**, 2095 (2003).
[5]M. E. Zoorob, M. D. B. Charleton, G. J. Parker, J. J. Baumberg, and M. C. Netti, Nature (London) **404**, 740 (2000).

[6]S. David, A. Chelnokov, and J. M. Lourtioz, Opt. Lett. **25**, 1001 (2000).
[7]C. Jin, B. Cheng, B. Man, Z. Li, and D. Zhang, Phys. Rev. B **61**, 10762 (2000).
[8]M. A. Kaliteevski, S. Brand, R. A. Abram, T. F. Krauss, P. Millar, and R. M. De La Rue, J. Phys.: Condens. Matter **13**, 10459 (2001).
[9]D. Sutter-Widmer, S. Deloudi, and W. Steurer, Phys. Rev. B **75**, 094304 (2007).
[10]K. Wang, Phys. Rev. B **76**, 085107 (2007).
[11]M. C. Rechtsman, H.-C. Jeong, P. M. Chaikin, S. Torquato, and P. J. Steinhardt, Phys. Rev. Lett. **101**, 073902 (2008).
[12]Y. Wang, X. Hu, X. Xu, B. Cheng, and D. Zhang, Phys. Rev. B **68**, 165106 (2003).
[13]K. Wang, Phys. Rev. B **73**, 235122 (2006).
[14]K. Mnaymneh and R. C. Gauthier, Optics Express **15**, 5089 (2007).
[15]K. Wang, Phys. Rev. B **82**, 045119 (2010).
[16]M. Bayindir, E. Cubukcu, I. Bulu, and E. Ozbay, Phys. Rev. B **63**, 161104(R) (2001).
[17]Y. Q. Wang, Z. F. Feng, X. S. Xu, B. Y. Cheng, and D. Z. Zhang, Europhys. Lett. **64**, 185 (2003).
[18]M. Notomi, H. Suzuki, T. Tamamura, and K. Edagawa, Phys. Rev. Lett. **92**, 123906 (2004).
[19]P.-T. Lee, T.-W. Lu, and F.-M. Tsai, IEEE Photonics Technol. Lett. **19**, 710 (2007).
[20]X. Xu, H. Chen, and D. Zhang, Appl. Phys. B **89**, 29 (2007).
[21]A. Micco, V. Galdi, F. Capolino, A. Della Villa, V. Pierro, S. Enoch, and G. Tayeb, Phys. Rev. B **79**, 075110 (2009).
[22]J. B. Pendry, J. Mod. Opt. **41**, 209 (1994).
[23]A. Moroz, Phys. Rev. Lett. **83**, 5274 (1999).
[24]J. B. Pendry, A. J. Holden, W. J. Stewart, and I. Youngs, Phys. Rev. Lett. **76**, 4773 (1996).
[25]G. Guida, D. Maystre, G. Tayeb, and P. Vincent, J. Opt. Soc. Am. B **15**, 2308 (1998).
[26]G. Guida, Opt. Commun. **156**, 294 (1998).
[27]J. W. Dong, G. Q. Liang, Y. H. Chen, and H. Z. Wang, Opt. Express **14**, 2014 (2006).
[28]L. Dal Negro, N. Feng, and A. Gopinath, J. Opt. A **10**, 064013 (2008).
[29]C. Forestiere, G. Miano, G. Rubinacci, and L. Dal Negro, Phys. Rev. B **79**, 085404 (2009).
[30]M. M. Bayindir, E. Cubukcu, I. Bulu, and E. Ozbay, Europhys. Lett. **56**, 41 (2001).
[31]C. Bauer, G. Kobiela, and H. Giessen, Phys. Rev. B **84**, 193104 (2011).
[32]Y. Wang, Opt. Express **16**, 1090 (2008).
[33]D. Gratias, A. Katz, and M. Quiquandon, J. Phys.: Condens. Matter **7**, 9101 (1995).
[34]H. Zhang and K. H. Kuo, Phys. Rev. B **42**, 8907 (1990).